A multifunctional organosilica cross-linker for the bio-conjugation of gold nanorods

Sarah Lai[a], Sonia Centi[a], Claudia Borri[a,b], Fulvio Ratto[a], Lucia Cavigli[a], Filippo Micheletti[a], Björn Kemper[c], Steffi Ketelhut[c], Tatiana Kozyreva[d], Leonardo Gonnelli[d], Francesca Rossi[a], Stefano Colagrande[b], Roberto Pini[a]*

[a] Institute of Applied Physics, National Research Council of Italy, Sesto Fiorentino, Italy
[b] Department of Experimental and Clinical Biomedical Science, University of Florence, Florence, Italy
[c] Biomedical Technology Center, University of Muenster, Muenster, Germany
[d] Giotto Biotech Srl, Sesto Fiorentino, Italy
**Corresponding author. Email address: f.ratto@ifac.cnr.it*

Abstract

We report on the use of organosilica shells to couple gold nanorods to functional peptides and modulate their physiochemical and biological profiles. In particular, we focus on the case of cell penetrating peptides, which are used to load tumor-tropic macrophages and implement an innovative drug delivery system for photothermal and photoacoustic applications. The thickness of organosilica exerts subtle effects on multiple parameters of the particles, including their size, shape, electrokinetic potential, photostability, kinetics of endocytic uptake and cytotoxicity, which are investigated by the interplay of colorimetric methods and digital holographic microscopy. As a rule of thumb, as the width of organosilica increases from none to ~ 30 nm, we find an improvement of the photophysical performances at the expense of a deterioration of the biological parameters. In principle, our synthetic protocols allow one to engineer this thickness with unique accuracy, which is a powerful asset to optimize or compromise on the parameters of interest for specific needs.

TOTAL NUMBER OF WORDS: 4859
TOTAL NUMBER OF TABLES: 0
TOTAL NUMBER OF FIGURES: 6

Keywords— Gold Nanorods, Organosilica shells, Cell Penetreting Peptides, Cytotoxicity of Nanoparticles, Cellular Uptake of Nanoparticles, Digital Holographic Microscopy

Introduction

In recent years, plasmonic particles as gold nanorods (GNRs), nanoshells, nanocages and a number of other shapes and clusters have come under examination as contrast agents for applications at the crossroads of nanomedicine and biomedical optics, including various photothermal and photoacoustic treatments to image and destroy cancer [1-8]. Gold nanoparticles combine good tolerability *in vivo* and, with respect to any organic dye, much better efficiency of optical absorbance. In particular, GNRs stand out from more standard gold nanospheres on account of the versatility of their plasmonic fingerprints, which are tunable across the whole near infrared (NIR) window and so allow one to reach solid tumors in depth.

To date, the systemic delivery of GNRs to tumors remains an outstanding issue. Upon intravenous injection, the mobility of gold nanoparticles is conditioned by a multitude of biological barriers [9]. Even after bio-labeling, these particles tend to spread among vital organs and accumulate into the liver and the spleen [6, 10, 11], with questionable effects in the long term. A radical alternative to this approach is to recruit tumor-tropic cells [12], such as macrophages, T cells, mesenchymal stem cells or neural stem cells, that may undertake the delivery of functional particles. In particular, macrophages seem to be an ideal option to take up gold nanoparticles [13-21], as their principal hallmark is to capture foreign bodies by endocytic pathways. Though lacking specificity for malignant cells, macrophages exhibit an innate tropism to trace gradients of signals released by necrotic and inflammatory tissue and are able to penetrate deep into the hypoxic core of solid tumors [22, 23].

The most standard approach to synthesize GNRs is to use cetrimonium bromide (CTAB) as a shape-directing agent and colloidal stabilizer [24-26]. However, CTAB-capped GNRs are cytotoxic and their aggregation into endocytic vesicles poses a threat to their optical

properties [11, 19, 27, 28], by the adverse effect of plasmonic coupling [29, 30]. The deposition of a rigid coating on CTAB-capped GNRs is one solution to overcome this problem. In particular, silanized GNRs prove to enjoy more optical stability upon aggregation and more photostability upon photothermal and photoacoustic conversion [19, 27, 29-35]. Indeed silica exerts much more protection than any soft coating may do, such as e.g. polystyrene sulfonate, polydiallyl dimethyl ammonium chloride or polyethylene glycol (PEG) [19, 27, 36-38]. In turn, these soft alternatives are unique to prevent flocculation in biological fluids or culture media and to provide stealth profile against the reticuloendothelial system. An additional advantage of functional PEG strands is their ease of modification with targeting units [33, 39-42]. Overall, the ideal is to combine the assets of a rigid coating, such as silica, with those of a soft one, such as PEG.

In fact, this architecture has already been demonstrated by other authors [27, 33, 41, 43]. However, it remains difficult to construct the interfaces between gold and silica and between silica and PEG step by step, because the affinity of these materials is rather poor. In an attempt to confine the deposition of silica around gold nanoparticles from tetraethyl orthosilicate, the use of CTAB [1, 32, 35, 41, 43-48] or PEG [19, 27, 31-33, 49] as templating agents has become a popular solution. Thereafter, the PEGylation of silanized particles has been conditioned to the deposition of a primer from another organosilane precursor in an intermediate step [27, 33, 41, 43]. Finally, PEGylated particles may be modified with targeting moieties [33, 41], such as bio or small ligands [10, 39, 40, 46, 50, 51]. In particular, peptides are attractive, owing to their small size, specificity, versatility, cost-effectiveness, scalability and biocompatibility.

Here, we introduce a novel approach to modify GNRs with organosilica, PEG and oligoarginine cell penetrating peptides (CPPs) [42], which serve, as an example, to promote the internalization of these particles into tumor-tropic cells. With respect to other methods to silanize GNRs, we believe that our protocol is more simple, robust and prone to additional

decoration, thus ensuring more reproducibility, yield and control over the deposition of silica. We exploit this advantage to prepare plasmonic particles with different thickness of the organosilica shells, which are left to interact with murine macrophages in order to realize tumor-tropic bio-vehicles. Here, we report on a critical comparison of the functional features of these systems, including their photostability, efficiency of endocytic uptake and cytotoxicity, in view of their delivery to solid tumors.

Materials and Methods

Materials: cetyltrimethylammonium bromide (CTAB), tetrachloroauric acid trihydrate ($HAuCl_4 \cdot 3H_2O$), sodium borohydride ($NaBH_4$), silver nitrate ($AgNO_3$), ascorbic acid, (3-mercaptopropyl) trimethoxysilane (MPS), sodium chloride (NaCl), 1-ethyl 3-(3-dimethylaminopropyl) carbodiimide (EDC), n-hydroxysuccinimide (NHS), 2-(n-morpholino)ethanesulfonic acid (MES), chitosan and WST-8 cell counting kit-8 were provided by Sigma-Aldrich and used without any other purification. Alpha-maleimido-omega-carboxy poly(ethylene glycol) (mal-PEG-COOH, MW ~ 5000) and alpha-mercapto-omega-carboxy poly(ethylene glycol) (HS-PEG-COOH, MW ~ 5000) were purchased from Iris Biothech (Germany). Dulbecco's Modified Eagle Medium (DMEM), fetal bovine serum, 1% L-glutamine and 1% penicillin-streptomycin solution were provided by BioWhittaker®, Lonza (Switzerland).

Synhesis of CPPs: Amino-modified CPPs were synthesized according to the sequence in ref. [42] and modified with an amino terminus.

Synthesis of GNRs: CTAB-capped GNRs were synthesized by the autocatalytic reduction of $HAuCl_4$ with ascorbic acid, according to the method proposed by Nikoobakht et al. [24] and modified by Ratto et al. [25], with the intent to consume the full aliquot of $HAuCl_4$ and gain more control over the total amount of gold in suspension.

Coating of GNRs with organosilica: Organosilica-coated GNRs (GNRs@sil) were prepared by a modification of the original procedure reported in ref [45]. After purification by two cycles of centrifugation and decantation, GNRs were transferred at a concentration of 800 µM Au in 200 µM aqueous CTAB at pH 10.5. Then, three aliquots of 1% or 5% MPS in isopropanol were added to these suspensions of GNRs, while stirring at a rate of 200 rpm, at intervals of 30 min, and left to react for 24 hrs at 37°C. The amount of MPS was varied within a molar ratio of Au / MPS between 0.08 and 2.7, in order to modulate the thickness of the deposition.

Bio-conjugation of organosilica-coated GNRs with CPPs: After coating with organosilica, these particles were washed to remove unreacted silanes by centrifugation and decantation. Pellets were re-dispersed in a non-saline 10 mM MES buffer at pH 6.5 and PEGylated by the addition of mal-PEG-COOH for 2 hrs at 37°C, until a molar ratio of mal-PEG-COOH / MPS of 10%. Alternatively, GNRs without organosilica were washed for three times by centrifugation, decantation and re-suspension in 500 µM aqueous CTAB, transferred into a saline (120 mM NaCl) 10 mM MES buffer at pH 6.5 and PEGylated by the addition of HS-PEG-COOH for 2 hrs at 37°C, as it is described in ref [36]. PEGylated organosilica-coated GNRs (GNRs@sil@PEG) and PEGylated GNRs without organosilica (GNRs@PEG) were purified by 5 cycles of centrifugation and decantation to remove unreacted PEG strands and residual CTAB used as a template for the deposition of organosilica.

GNRs@sil@PEG or GNRs@PEG at a concentration of 1.6 mM Au in a saline 10 mM MES buffer at pH 5.5 were activated by the addition of an equal volume of the same MES buffer containing 12 mM NHS and 48 mM EDC for 15 min at 37°C. Finally, a double volume of the same MES buffer containing 20 ppm of amino-terminated CPPs was added, in order to achieve their conjugation by amidation. Bio-conjugated organosilica-coated GNRs (GNRs@sil@PEG@CPP) and bio-conjugated GNRs without organosilica (GNRs@PEG@CPP) were purified by three cycles of centrifugation with a dead volume ratio

of ~ 1/200, transferred at a nominal concentration of 4.0 mM Au into sterile PBS and stored at 4°C for no more than one week.

In this study, we compare GNRs coated with 5 or 30 nm of organosilica, PEGylated and bio-conjugated with CPPs (samples S5 or S30, respectively, the thickness of organosilica being expressed in terms of hydrodynamic size) and GNRs without organosilica, PEGylated and bio conjugated with CPPs (sample S0).

Through all steps from CTAB-coated GNRs to GNRs@sil@PEG@CPP or GNRs@PEG@CPP, suspensions were characterized by UV-NIR spectrophotometry, transmission electron microscopy and dynamic light scattering. Spectra of optical extinction were acquired with a V-560 spectrophotometer from Jasco, Japan, by using quartz cuvettes with optical pathlength of 1 cm. Morphological details were retrieved with a CM12 transmission electron microscope (TEM) from Philips, the Netherlands, with a voltage of 100 kV and operating in standard conditions. Samples were prepared for TEM inspection by dripping on carbon-holey or carbon-copper films. Hydrodynamic sizes and electrokinetic potentials were measured with a Zetasizer Nano-ZS90 from Malvern Instruments, UK, at 25 °C and by averaging over three sets of 15 runs each, at a scattering angle of 90°.

Photoacoustic measurements: the photostability was measured by the photoacoustic (PA) method that is described in detail in ref [52, 53]. In brief, hybrid films of chitosan containing homogeneous distributions of the various particles were directed to a home-made PA microscope featuring an optical parametric oscillator pumped with the third harmonic of a Nd:YAG Q-switched laser. Each film was irradiated in different points with 20 light pulses at different optical fluences (F). Average PA signals over 200 light pulses at an optical fluence of 1 mJ/cm^2, which is well below the onset of photoinstability, were compared in each point before and after irradiation at F, in order to detect alterations in the efficiency of PA conversion.

Cell line and culture conditions: J774A.1 murine macrophages were seeded on plastic Petri dishes in Dulbecco's Modified Eagle Medium (DMEM) supplemented with 10% fetal bovine serum, 1% L-glutamine and 1% penicillin-streptomycin solution. Cells were kept and left to grow under standard conditions (37°C, 5% CO_2, 100% relative humidity).

Cytotoxicity assay: 8×10^3 macrophages were cultured in 96-well plates and incubated with the various particles at concentrations in the range of 50 to 400 μM Au, for incubation times of 4, 24 and 48 hrs. Each sample was prepared in triplicate. Cellular viability was evaluated by WST-8 assay, which exploits the reduction of the highly water-soluble tetrazolium salt WST-8 by cellular dehydrogenases into the yellow dye formazan. The optical absorbance of formazan at 460 nm is proportional to the number of living cells and was measured with a plate reader**.** Data were expressed as the percentage of optical absorbance at 460 nm with respect to relevant controls.

Cellular uptake: The accumulation in macrophages was quantified by an optical analysis. 5×10^5 macrophages were plated in Petri dishes and treated with the various particles at concentrations of 100 and 400 μM Au, for incubation times of 4, 8, 16, 24, 32 and 48 hrs. Macrophages were harvested, washed with PBS and fixed with a solution of 3.6% paraformaldehyde in PBS for 10 min at room temperature. Then, samples were washed, re-suspended in 120 μL of PBS in a quartz microcuvette and directed to a UV-NIR spectrophotometer (V-560, Jasco, Japan). The spectra of optical extinction were modeled as the sum of an empirical background from a population of macrophages plus a numerical approximation of the plasmonic band from a colloid of GNRs. The latter was described as an integral over Gans lineshapes [26], by using the dielectric function of gold by Etchegoin et al. [54]. Details of this method are provided elsewhere [39, 55].

Digital holographic microscopy (DHM): an inverted microscope (iMIC from Till Photonics, Graefelfing, Germany) equipped with a DHM module was applied for bright field imaging and quantitative phase contrast imaging. Macrophages were seeded in Petri dishes, incubated

with the various particles, washed and fixed with a solution of 3.6% paraformaldehyde in PBS for 10 minutes at room temperature. The DHM analysis was performed under PBS at room temperature [56].

In brief, the source of coherent light was a frequency-doubled Nd:YAG laser (Coherent Compass 315M, Coherent, Luebeck, Germany, λ = 532 nm). Digital off-axis holograms of macrophages were recorded at random locations with a 20× objective lens (Zeiss LD Achroplan 20×/0.4 Korr, NA = 0.4, Carl Zeiss, Goettingen, Germany), by using a custom-built C^{++} software. The numerical reconstruction of digitally captured holograms was performed by spatial phase shifting in combination with optional holographic autofocusing [56-59]. From quantitative DHM phase-contrast images, the average area covered by single cells, the cell number and the cell-induced average phase contrast were determined by image segmentation with a freeware cell profiler [60]. Moreover, from these parameters, the average dry mass per cell was calculated, as it is described in ref [61].

Results and Discussion

Physiochemical parameters of the particles: Figure 1b displays the zeta potential of CTAB-capped GNRs and their subsequent modifications with organosilica, PEG and CPPs. Initially, GNRs display a cationic profile, due to the presence of CTAB. A net positive charge is maintained even after CTAB-templated silanization and is inverted only after PEGylation with mal-PEG-COOH. This inversion is ascribed to the combination of a loss of CTAB from the mesopores of organosilica upon centrifugation purification [45] and the addition of the carboxylic functions from mal-PEG-COOH. When CPPs are added, the zeta potential increases by several mV, which is consistent with the presence of these polycationic species [42]. All these trends were also more qualitatively confirmed by the use of electrophoresis (data not shown).

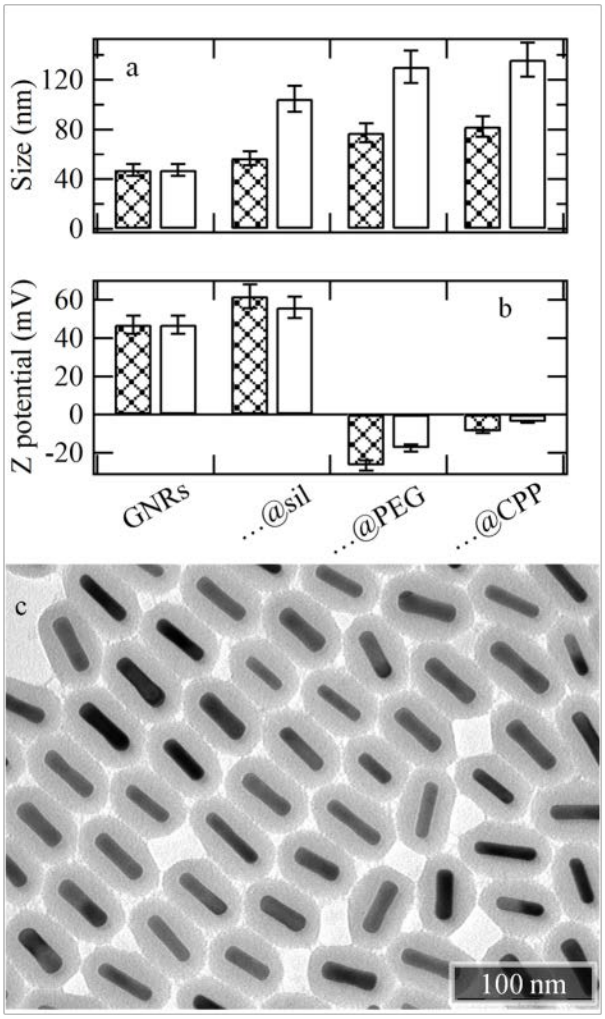

Figure 1. (***a***) Hydrodynamic diameter and (***b***) electrokinetic potential though the various steps of the preparation of samples S5 (crossed fill) and S30 (white fill). (***c***) Representative TEM micrograph of sample S30.

The average size of CTAB-capped GNRs, as measured by TEM and in agreement with DLS is 47 nm × 12 nm (length × diameter), with an average aspect ratio around 4. Upon coating with organosilica, their hydrodynamic size increases up to 57 nm and 100 nm, respectively for samples S5 and S30 (see **Fig. 1a**). In both samples, as well as in sample S0 (data not shown), another ~ 20 nm and ~ 5 nm are added after PEGylation and bio-conjugation with CPPs, respectively. The TEM micrograph in **Fig. 1c** demonstrates the effectiveness of this method to coat CTAB-capped GNRs with a uniform shell of organosilica.

CTAB-capped GNRs prepared by seed-mediated methods were used for encapsulation with porous silica by different authors [1, 32, 35, 41, 43-48]. The development of simple and

robust protocols to coat plasmonic particles has received great interest, as a means to enhance their optical stability against aggregation [19, 27, 29, 30], their photostability against optical excitation [31-35, 62], their capability to load drugs [41, 46, 47, 49] or to gain hydrophobicity [63]. Most of previous work rested on a direct implementation of Stöber method to coat CTAB-capped GNRs with porous silica. This method consists of the hydrolysis and condensation of a tetravalent precursor of silica, usually in the pool of alkoxy-silanes, in an alkaline environment and in the presence of an excess of CTAB. The latter serves to ensure a dense bilayer around the gold cores, foster the confinement of silica and maintain a net positive charge throughout the reaction. However, too much free or micellar CTAB in solution may initiate extra nuclei at the detriment of the confinement of silica and so the dosage of CTAB is stringent [46, 47] and causes irreproducibility. Conversely, our approach requires lesser CTAB, as it is the chemical affinity between mercapto-silanes and gold that governs the confinement of silica at the stage of nucleation, thus improving the yield and control over the reaction. However, its total elimination is unfeasible, because CTAB does not only serve as a templating agent, but also as a colloidal stabilizer that maintains the cationic profile throughout the reaction .

To the best of our knowledge, the use of functional organosilanes alone, such as MPS, to produce thick shells of organosilica around CTAB-capped GNRs has never been reported before. Mercaptans [64-67] or amines [68] have been proposed as primers, but the deposition of thicker shells of silica is mostly committed to the addition of tetraethyl orthosilicate or other tetravalent precursors. Our protocol provides for fine control over the thickness of organosilica as well as a high density of functional groups for subsequent modification. Indeed, another key advantage of MPS is its ease of bio-conjugation with thiol-reactive moieties in one step, such as maleimide esters. Here, we exploited this feature to add mal-PEG-COOH. PEGylation provides for biomimicry and unique colloidal stability in saline

buffers for cell biology, which enables a safe removal of CTAB and so improves the biocompatibility of the final product [27, 36-38].

After silanization, PEGylation and bio-conjugation, all particles maintained their optical properties (see **Fig. S1** in SI) and, while the transverse band around 512 nm remained almost there, the longitudinal band underwent a significant red-shift. This is a typical outcome of an increase in the refractive index of the dielectric medium surrounding the plasmonic core, as it is due to the formation of silica. The effect proceeds as the shell becomes thicker, in agreement with refs. [26, 29, 35, 43, 63, 67, 69]. For instance, for samples S5 and S30, we found a red-shift of the longitudinal band by about 5 and 40 nm, respectively.

A decisive merit of silanization is its ability to enhance the photostability of GNRs in a regime of interest for PA imaging [31-34]. Here, we assessed this parameter for samples with different thickness of organosilica, by the use of the method in ref [52, 53]. The decrease of the efficiency of PA conversion at the probe fluence of 1 mJ/cm^2 after irradiation with a certain excitation fluence (F) provides direct evidence for irreversible changes in the optical absorbance of the samples, which is ascribed to a reshaping of the GNRs toward rounder particles [52, 55]. This decrease is quantified by measuring the ratio R between the PA signals at the probe fluence after and before irradiation at F. In practice, a threshold for the onset of photoinstability is defined as the smallest value of F that corresponds to a value of R below unity. **Figure 2** shows the trend of R as a function of F. A clear pattern to the thickness of organosilica is observed (see **Table S1** in SI). The thicker the shells the higher the thresholds, with an increase from 2.5 mJ/cm^2 for sample S0 to 6.5 mJ/cm^2 for sample S30. An enhancement of the photostability and thermal stability of gold nanorods after silanization has been observed by different authors, both in a continuous regime of thermal treatment [35, 44, 70] and upon optical excitation with ns-[31-34] as well as fs-[62] long pulses. However, to our knowledge, our approach provides for the first quantitative definition of a threshold fluence, which seems to roughly improve by as much as ~10% per nm of shell thickness.

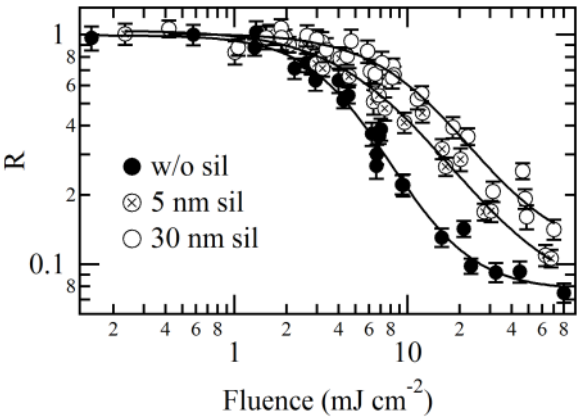

Figure 2. Relative efficiency of photoacoustic conversion after optical excitation at different fluences, expressed as ratio R of the intensities of the photoacoustic signals taken after and before irradiation at different fluences (see the main text for details).

Cellular uptake of the particles: Cellular uptake was investigated in murine macrophages, which are taken as a representative model of tumor-tropic cells [13-20]. Samples S0, S5 and S30 were exposed to these cells at concentrations of 100 and 400 μM Au for incubation times between 4 and 48 hrs. **Figures 3a**, **b** and **c** display their experimental spectra of optical extinction, together with their numerical analysis, for the concentration of 400 μM Au.

While macrophages treated with PEGylated GNRs without CPPs do not exhibit any detectible plasmonic band [36], owing to the stealth profile of PEG [27, 36-38], their bio-conjugation with CPPs triggers a dramatic enhancement of their cellular uptake. We note that the shape of the longitudinal band in sample S0 undergoes some deterioration for incubation times exceeding 24 hrs, which is attributed to the onset of plasmonic coupling in the absence of a rigid spacer [29, 30]. Instead, a shell of organosilica as thin as 5 nm is sufficient to remove this effect, as it is seen in sample S5, at all incubation times. Conversely, the shape of the plasmonic band is intact in sample S30, but its overall intensity undergoes a significant loss with respect to its counterparts with lesser or no silica. These findings are essentially consistent with those in refs [19, 27], where a shell of silica was used to protect the optical

features of GNRs upon aggregation in biological samples. Here, we note that sample S0 does clearly suffer from some plasmonic coupling, but its soft shell of PEG and CPPs is already quite sufficient to avoid catastrophic effects, such as those observed in anhydrous biopolymers [29, 30]. Similar findings were reported with different ligands [39] or different polymers, such as polystyrene sulfonate and polyallylamine hydrochloride [19].

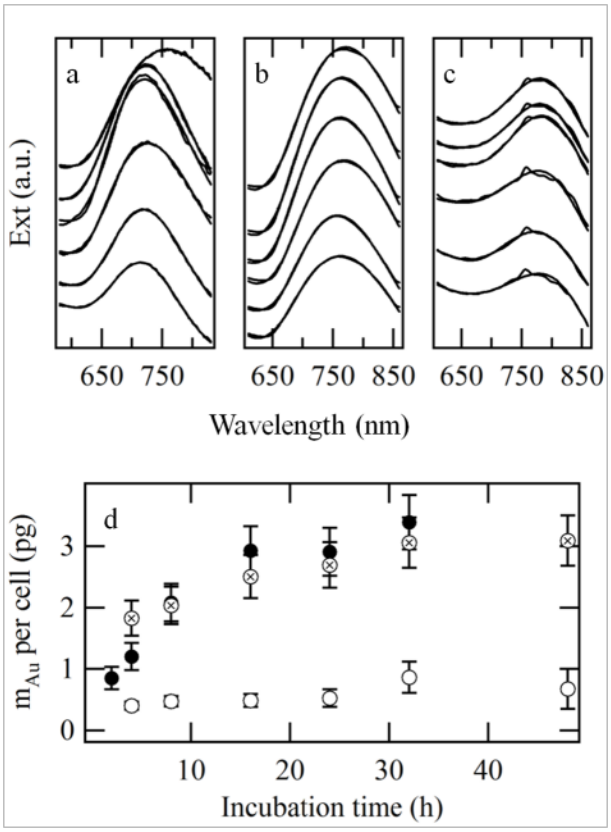

Figure 3. Spectra of optical extinction from macrophages treated with samples S0 (***a***), S5 (***b***) and S30 (***c***) at 400 µM Au for 4, 8, 16, 24, 32 and 48 hrs, from bottom to top. The experimental datapoints are overlapped with their numerical model, as it is mentioned in the main text. Results are displayed in panel (***d***) in terms of mass of Au per cell for samples S0 (black fill), S5 (crossed fill) and S30 (white fill).

The overall level of cellular uptake depends on the thickness of organosilica, the concentration of gold in suspension and incubation time (**Figure 3d**). The mass of gold per cell increases with concentration and incubation time, until saturation after ~ 32 hrs. Thereafter, we hypothesize that endocytic and exocytic processes may reach an equilibrium [71-73]. Instead,

the pattern to the thickness of organosilica is less obvious. Samples S0 and S5 are similar already after 4 hrs. In the presence of a thin shell of organosilica, the mass of gold per cell seems to be a little higher at shorter incubation times and to saturate a little earlier to a value in the order of 2 – 3 pg Au, already after about 12 hrs. In contrast, the mass of gold per cell in the case of sample S30 reaches a value that is about 3 times lower than those of cases S0 and S5, although this measurement suffers from more fluctuations over time. This observation is qualitatively confirmed by the DHM images in **Fig. 4**. Macrophages loaded with samples S0 and S5 are similar and contain a greater amount of dark vesicles, as compared to sample S30.

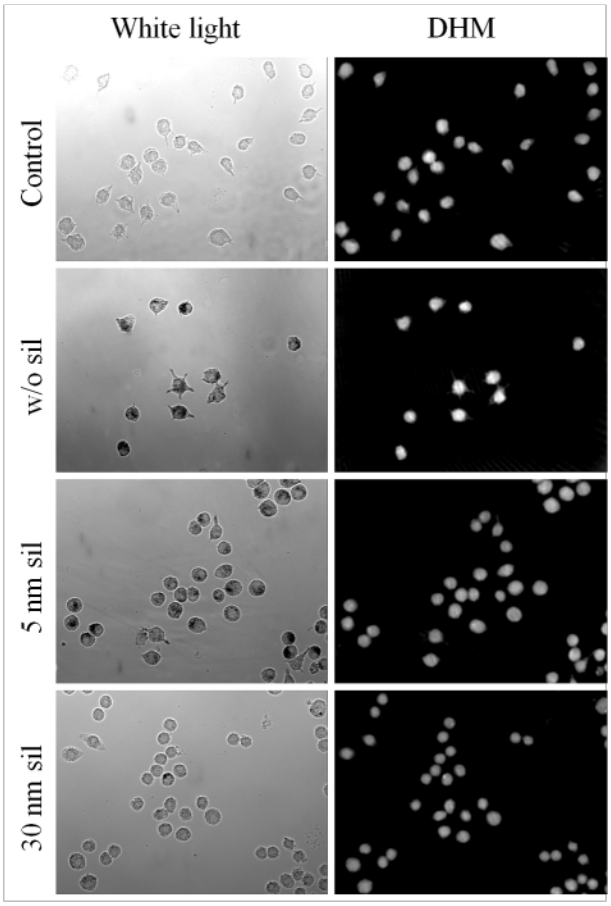

Figure 4. (***a***) White light and (***b***) DHM quantitative images of macrophages treated with samples S0 (w/o sil), S5 (5 nm sil) and S30 (30 nm sil) at 400 μM Au for 24 hrs.

Viability of the cellular vehicles: The cytotoxicity of samples S0, S5 and S30 was studied as a function of the concentration of gold in suspension and incubation time by a WST-8 assay.

Sample S5 exhibits a good cellular viability, similar to its counterpart without silica [36], through the full range of incubation times, except for the data point at the concentration of 400 μM Au at 48 hrs (**Figures 5a** and **b**). Also sample S30 exhibits fair atoxicity until 24 hours. However, for longer incubation times, these particles start to become more cytotoxic, even if their IC50 still remains above 400 μM Au.

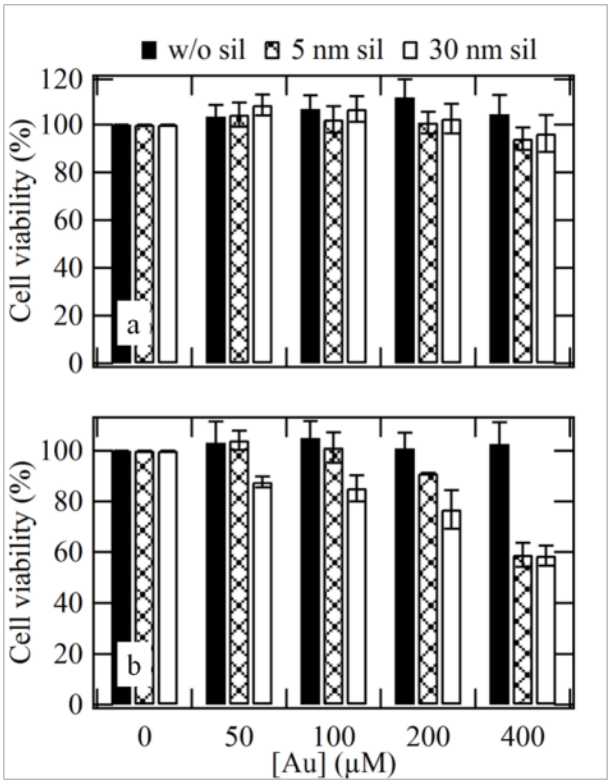

Figure 5. Cytotoxicity of samples S0 (black fill), S5 (crossed fill) and S30 (white fill) on macrophages, in the range of concentrations between 50 to 400 μM Au after 24 (***a***) and 48 (***b***) hrs. Data are expressed as percent of controls. All essays were made in triplicate.

These data are confirmed by the use of bright field microscopy and DHM for samples S0, S5 and S30 at the concentrations of 100 and 400 μM Au, upon incubation with macrophages for 24 hrs (see **Figure 6**). The presence of organosilica, both in samples S5 and S30, does not

seem to alter much the morphology of these cells, as compared with the effect in the absence of silica [36] and blank controls. **Figure 6a** shows that the average dry mass of individual cells remains normal. Therefore, the intracellular content of proteins, DNA, RNA, etc. does not undergo detectible variations, which is a sensitive indication for atoxicity [61]. Instead, the surface area per cell in **Fig. 6b** highlights some stress, which increases with the thickness of organosilica and correlates with the evidence from the WST-8 assay.

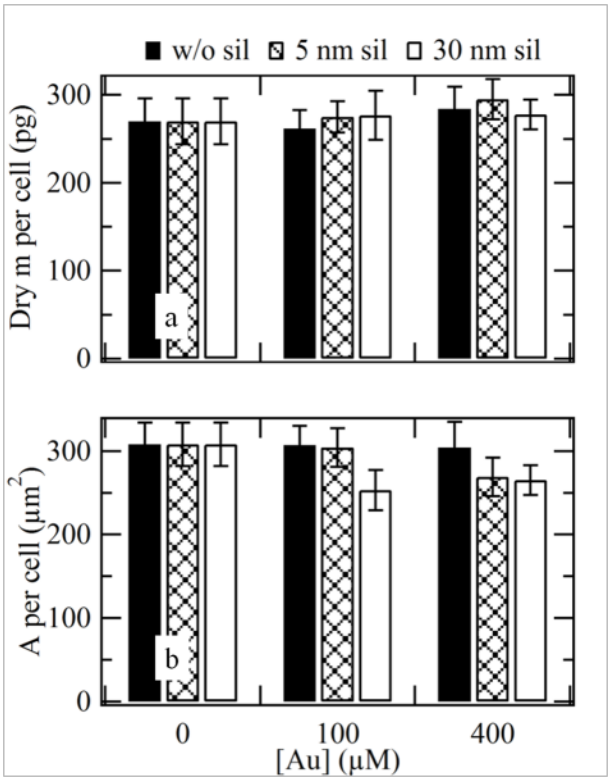

Figure 6. (***a***) Dry mass per cell and (***b***) average surface area covered by a single cell for macrophages treated with samples S0 (black fill), S5 (crossed fill) and S30 (white fill) at 100 and 400 μM Au for 24 hrs. All essays were made in triplicate.

For the preparation of cellular vehicles, it is critical that the biological functions of tumor-tropic cells remain intact [12]. We conjecture that the residual cytotoxicity for sample S30 may be ascribed to a larger pore volume, which entails the adsorption of more CTAB. The release of free CTAB is considered to be the key party for the residual cytotoxicity of GNRs, by disintegrating bio-membranes and peptides even at micromolar concentrations [36, 74-77].

In this study, CTAB was used in the synthesis of GNRs and their silanization, in order to maintain the colloidal stability throughout the reaction. Although as many as 8 cycles of centrifugation, decantation and re-dispersion in aqueous buffers were carried out to eliminate any CTAB and other reagents [45], we hypothesize that it is its residual adsorbate to affect the cellular viability for thicker shells and incubation times exceeding 24 hrs.

Overall, we note that samples S0, S5 and S30 only differ by the thickness of organosilica, i.e. their hydrodynamic size and electrokinetic potential. The comparison of their photostability in **Table S1** highlights the merit of a thicker shell. Instead, as it is seen in the spectra of optical extinction in **Figs. 3a**, **b** and **c**, a shell thicker than a few nm becomes redundant in terms of optical stability against aggregation and deleterious in terms of cellular uptake, probably due to its steric hindrance and contamination. Instead, a thin shell of silica, in the order of 5 nm, combines excellent optical stability and efficient cellular uptake. **Figs. 5** and **6** show that the thicker the shell, the worse the cytotoxicity of these particles, although the effect is quite subtle and the cellular viability remains above 90% of control until a concentration of 400 μM Au and an incubation time of 24 hrs in all cases, which is long enough to saturate the capacity of these cellular vehicles, according to **Fig. 3d**.

Conclusions

We have reported on a hybrid architecture of plasmonic particles that are coated with organosilica, PEG and ligands, such as CPPs of interest for the preparation of cellular vehicles with a tumor-tropic profile. We have developed a convenient and robust procedure to coat single GNRs with organosilica and gain more control over its thickness and the prospect of click bio-conjugation, by the use of mercaptosilanes. We have capitalized on this versatility to compare the physiochemical and biological profiles of three samples with different thickness of organosilica, i.e. 0 nm (S0), 5 nm (S5) and 30 nm (S30). The use of CPPs with a

polycationic chain was taken as a case to foster the internalization of all samples into macrophages.

The optical absorbance of all particles maintains the typical plasmonic features of GNRs, which red-shift more and more with the thickness of organosilica, say at a rate of 1 nm per nm of shell width for a longitudinal band around 800 nm. Moreover, we have confirmed that the shell enhances the photostability of these particles, roughly by 10% per nm of organosilica. With respect to sample S0, the optical thresholds to damage sample S30 are about 2.5 times higher. However, the cellular uptake of these particles becomes less efficient, supposedly due to their steric hindrance and residual contamination. The mass of Au per cell drops from about 3 pg in samples S0 and S5 to several hundred fg for sample S30 after about 24 hrs in the presence of 400 μM Au. Besides, both samples S5 and S30 prevent the slight loss of optical stability that is observed in sample S0, upon segregation in endocytic vesicles. The cellular viability of macrophages that are incubated with these samples remains around 95 – 99% of controls in all cases up to 24 hrs and concentrations of 200 μM Au. For longer incubation times and higher concentrations, some cytotoxicity arises and correlates with the thickness of organosilica, probably due to a slow release of the residual adsorbate of CTAB.

In conclusion, a shell of organosilica with a thickness of a few nm seems to be an excellent compromise in view of the incorporation of plasmonic particles into cellular vehicles. A thicker shell provides for more photostability at the expense of a lesser efficiency of cellular uptake and a more problematic detoxication. On the other hand, in the absence of a rigid shell, these particles lose photostability and optical stability against aggregation. In the future, we wish to refine our protocols to remove the residual adsorbate of CTAB from the mesopores of organosilica and extend our biological investigations by the assessment of additional parameters, such as the chemotactic behavior of the macrophages, and the translation to more kinds of functional cells for applications in cancer therapy and cell tracking.

This work was in part supported by the Project of Tuscan Region “SYNERGY” and by the ERANET+ Project of Tuscan Region and European Community “LUS BUBBLE”.

References

[1] B. Gao, J. Xu, K. W. He, L. Shen, H. Chen, H. J. Yang, A. Li, W. Xiao, Cellular uptake and intra-organ biodistribution of functionalized silica-coated gold nanorods, Mol Imaging Biol 18(5) (2016) 667-676

[2] X. Yang, M. Yang, B. Pang, M. Vara, Y. Xia, Gold nanomaterials at work in biomedicine, Chem Rev 115(19) (2015) 10410-10488

[3] W. Choi, A. Sahu, Y. H. Kim, G. Tae, Photothermal cancer therapy and imaging based on gold nanorods, Ann Biomed Eng 40(2) (2012) 534-546

[4] E. C. Dreaden, A. M. Alkilany, X. H. Huang, C. J. Murphy, M. A. El-Sayed, The golden age: gold nanoparticles for biomedicine, Chem Soc Rev 41(7) (2012) 2740-2779

[5] B. N. Khlebtsov, E. V. Panfilova, G. S. Terentyuk, I. L. Maksimova, A. V. Ivanov, N. G. Khlebtsov, Plasmonic nanopowders for photothermal therapy of tumors, Langmuir 28(24) (2012) 8994-9002

[6] L. C. Kennedy, L. R. Bickford, N. A. Lewinski, A. J. Coughlin, Y. Hu ,E. S. Day , J. L. West, R. A. Drezek, A new era for cancer treatment: gold-nanoparticle-mediated thermal therapies, Small 7(2) (2011) 169-183

[7] F. Ratto, P. Matteini, S. Centi, F. Rossi, R. Pini, Gold nanorods as a new nanochromophores for photothermal terapies, J Biophotonics 4(1-2) (2011) 64-73

[8] P. K. Jain, I. H. El-Sayed, M. A. El-Sayed, Au nanoparticles target cancer, Nano Today 2(1) (2007) 18-19

[9] S. K. Sriraman, B. Aryasomayajula, V. P. Torchilin, Barriers to drug delivery in solid tumors, Tissue Barriers 2 (2014) e29528

[10] X. Huang, X. Peng, Y. Wang, Y. Wang, D. M. Shin, M. A. El Sayed, S. Nie, A reexamination of active and passive tumor targeting by using rod-shaped gold nanocrystals and covalently conjugated peptide ligands, ACS Nano 4(10) (2010) 5887-5896

[11] N. Khlebtsov, L. Dykman, Biodistribution and toxicity of engineered gold nanoparticles: a review of in vitro and in vivo studies, Chem Soc Rev 40(3) (2011) 1647-1671

[12] S. Tan, T. Wu, D. Zhang, Z. Zhang, Cell or cell membrane-based drug delivery systems, Theranostics 5(8) (2015) 863-881

[13] F. Ratto, S. Centi, C. Avigo, C. Borri, F. Tatini, L. Cavigli, C. Kusmic, B. Lelli, S. Lai, S. Colagrande, F. Faita, L. Menichetti, R. Pini, A robust design for

cellular vehicles of gold nanorods for multimodal imaging, Adv Funct Mater 26(39) (2016) 7178-7185

[14] A. J. Trinidad, S. J. Hong, Q. Peng, S. J. Madsen, H. Hirschberg, Combined concurrent photodynamic and gold nanoshell loaded macrophage-mediated photothermal therapies: An in vitro study on squamous cell head and neck carcinoma, Lasers Surg. Med. 46(4) (2014) 310-318

[15] M. R. Choi, R. Bardhan, K. J. Stanton-Maxey, S. Badve, H. Nakshatri, K. M. Stantz, N. Cao, N. J. Halas, S. E. Clare, Delivery of nanoparticles to brain metastases of breast cancer using a cellular Trojan horse, Cancer Nano 3(1-6) (2012) 47-54

[16] S. J. Madsen, S. K. Baek, A. R. Makkouk, T. Krasieva, H. Hirschberg, Macrophages as cell-based delivery systems for nanoshells in photothermal therapy, Ann Biomed Eng 40(2) (2012) 507-515

[17] T. D. Yang, W. Choi, T. H. Yoon, K. J. Lee, J. S. Lee, S. H. Han, M. G. Lee, H. S. Yim, K. M. Choi, M. W. Park, Real-time phase-contrast imaging of photothermal treatment of head and neck squamous cell carcinoma: an in vitro study of macrophages as a vector for the delivery of gold nanoshells, J Biomed Opt 17(12) (2012) 128003

[18] M. R. Choi, K. J. Stanton-Maxey, J. K. Stanley, C. S. Levin, R. Bardhan, D. Akin, S. Badve, J. Sturgis, J. P. Robinson, R. Bashir, N. J. Halas, S. E. Clare, A cellular Trojan horse for delivery of therapeutic nanoparticles into tumors, Nano Lett 7(12) (2007) 3759-3765

[19] P. P. Joshi, S. J. Yoon, Y.-S. Chen, S. Emelianov, K. V. Sokolov, Development and optimization of near-IR contrast agents for immune cell tracking, Biomed Opt Exp 4 (11) (2013) 2609-2618

[20] Z. Li, H. Huang, S. Tang, Y. Li, X.-F. Yu, H. Wang, P. Li, Z.Sun, H. Zhang, C. Liu, P. K. Chu, Small gold nanorods laden macrophages for enhanced tumor coverage in photothermal therapy, Biomaterials 74 (2016) 144-154

[21] G. Baldi, C. Ravagli, M. Comes Franchini, M. M. D'Elios, M. Benagiano, M. Bitossi, Magnetic nanoparticles functionalized with cathecol, production and use thereof, (Colorobbia Italia S.p.A.) WO 104664 (2015).

[22] R. Noy, J. W. Pollard, Tumor-associated macrophages: from mechanisms to therapy, Immunity 41(1) (2014) 49-61

[23] P. Chiarugi, Cancer-associated fibroblasts and macrophages, Oncoimmunology 2(9) (2013) e25563

[24] B. Nikoobakht, M. A. El-Sayed, Preparation and growth mechanism of gold nanorods (NRs) using seed-mediated growth method, Chem Mater 15(10) (2003) 1957-1962

[25] F. Ratto, P. Matteini., F. Rossi, R. Pini, Size and shape control in the overgrowth of gold nanorods, J Nanopart Res 12(6) (2010) 2029-2036

[26] J. Pérez-Juste, I. Pastoriza-Santos, L. M. Liz-Marzán, P. Mulvaney. Gold nanorods: synthesis, characterization and applications, Coord Chem Rev 249(17-18) (2005) 1870-1901

[27] Y. Akiyama, Y. Niidome, T. Mori, Y. Katayama, T. Niidome, PEG-silica-modified gold nanorods that retain their optical properties in tumor tissues, J Biomater Sci Polym Ed 24(18) (2013) 2071-2080

[28] C. Ungureanu, R. Kroes, W. Petersen, T. A. M. Groothuis, F. Ungureanu, H. Janssen, F. W. B. van Leeuwen, R. P. H. Kooyman, S. Manohar, T. G. van Leeuwen, Light interactions with gold nanorods and cells: implications for photothermal nanotherapeutics, Nano Lett 11(5) (2011) 1887-1894

[29] M. Mazzoni, F. Ratto, C. Fortunato, S. Centi, F. Tatini, R. Pini, Partial decoupling in aggregates of silanized gold nanorods, J Phys Chem C 118(34) (2014) 20018-20025

[30] M. Mazzoni, F. Ratto, C. Fortunato, S. Centi, R. Pini, Basic sets for plasmonic diagnostics in aggregates of capped and uncapped gold nanorods, Plasmonics 10(1) (2015) 9-15

[31] Y. S. Chen, W. Frey, S. Kim, K. Homan, P. Kruizinga, K. Sokolov, S. Emelianov, Enhanced thermal stability of silica-coated gold nanorods for photoacoustic imaging and image-guided therapy, Opt Express 18(9) (2010) 8867-8878

[32] Y. S. Chen, W. Frey, S. Kim, P. Kruizinga, K. Homan, S. Emelianov, Silica-coated gold nanorods as photoacoustic signal nanoamplifiers, Nano Lett 11(2) (2011) 348-354

[33] X. Hu, X. Gao, Multilayer coating of gold nanorods for combined stability and biocompatibility, Phys Chem Chem Phys 13(21) (2011) 10028-10035

[34] L. C. Chen, C. W. Wei, J. S. Souris, S. H. Cheng, C. T. Chen, C. S. Yang, P. C. Li, L. W. Lo, Enhanced photoacoustic stability of gold nanorods by silica matrix confinement, J Biomed Opt 15(1) (2010) 016010

[35] J. Liu, C. Kan, B. Cong, H. Xu, Y. Ni, Y. Li, D. Shi, Plasmonic property and stability of core-shell Au@SiO2 nanostructures, Plasmonics 9 (2014) 1007-1014

[36] F. Tatini, I. Landini, F. Scaletti, L. Massai, S. Centi, F. Ratto, S. Nobili, G. Romano, F. Fusi, L. Messori, E. Mini, R. Pini, Size dependent biological profiles of PEGylated gold nanorods, J Mater Chem B 2 (2014) 6072-6080

[37] M. Eghtedari, A. Oraevsky, J. A. Copland, N. A. Kotov, A. Conjusteau, M. Motamedi, High sensitivity of in vivo detection of gold nanorods using a laser optoacoustic imaging system, Nano Lett 7(7) (2007) 1914-1918

[38] T. Niidome, M. Yamagata, Y. Okamoto, Y. Akiyama, H. Takahashi, T. Kawano, Y. Katayama, Y. Niidome, PEG-modified gold nanorods with a stealth character for in vivo applications, J Control Release 114(3) (2006) 343-347

[39] F. Ratto, E. Witort, F. Tatini, S. Centi, L. Lazzeri, F. Carta, M. Lulli, D. Vullo, F. Fusi, C. T. Supuran, A. Scozzafava, S. Capaccioli, R. Pini, Plasmonic particles that hit hypoxic cells, Adv Funct Mater 25(2) (2015) 5316-5323

[40] S. Centi, F. Tatini, F. Ratto, A. Gnerucci, R. Mercatelli, G. Romano, I. Landini, S. Nobili, A. Ravalli, G. Marrazza, E. Mini, F. Fusi, R. Pini, In vitro assessment of antibody-conjugated gold nanorods for systemic injections, J Nanobiotech 12 (2014) 55

[41] S. Shen, H. Tang, X. Zhang, J. Ren, Z. Pang, D. Wang, H. Gao, Y. Qian, X. Jiang, W. Yang, Targeting mesoporous silica-encapsulated gold nanorods for chemo-photothermal therapy with near-infrared radiation, Biomater 34(12) (2013) 3150-3158

[42] E. Oh, J. B. Delehanty, K. E. Sapsford, K. Susumu, R. Goswami, J. B. Blanco-Canosa, P. E. Dawson, J. Granek, M. Shoff, Q. Zhang, P. L. Goering, A. Huston, I. L. Medintz, Cellular uptake and fate of PEGylated gold nanoparticles is dependent on both cell-penetration peptides and particle size, Acs Nano 5(8) (2011) 6434-6448

[43] W. C. Wu, J. B. Tracy, Large-scale silica overcoating of gold nanorods with tunable shell thicknesses, Chem. Mater. 27 (2015) 2888-2894

[44] E. Gergely-Fülöp, D. Zámbó, A. Deák, Thermal stability of mesoporous silica-coated gold nanorods with different aspect ratios, Mater Chem Phys 148(3) (2014) 909-913

[45] I. Gorelikov, N. Matsuura, Single-step coating of mesoporous silica on cetyltrimethyl ammonium bromide-capped nanoparticles, Nano Lett 8(1) (2008) 369–373

[46] Q. Zhan, J. Qian, X. Li, S. He, A study of mesoporous silica-encapsulated gold nanorods as enhanced light scattering probes for cancer cell imaging, Nanotechnology 21(5) (2009) 055704

548 [47] Z. Zhang, L. Wang, J. Wang, X. Jiang, X. Li, Z. Hu, Y. Ji, X. Wu, C. Chen,
549 Mesoporous silica-coated gold nanorods as a light-mediated multifunctional
550 theranostic platform for cancer treatment, Adv Mater 24(11) (2012) 1418-1423

551 [48] C. Wang, Z, Ma, T. Wang, Z. Su, Synyhesis, assembly, and
552 biofunctionalization of silica-coated gold nanorods for colorimetric biosensing, Adv
553 Funct Mater 16 (2006), 1673-1678

554 [49] G. Terentyuk, E. Panfilova, V. Khanadeev, D. Chumakov, E. Genina, A.
555 Bashkatov, V. Tuchin, A. Bucharskaya, G. Maslyakova, N. Khlebtsov, B. Khlebtsov,
556 Gold nanorods with a hematoporphyrin-loaded silica shell for dual-modality
557 photodynamic and photothermal treatment of tumors in vivo, Nano Res 7 (3) (2014)
558 325-337

559 [50] P. Nativo, I. Prior, M. Brust, Uptake and intracellular fate of surface-modified
560 gold nanoparticles, ACS Nano 2(8) (2008) 1639-1644

561 [51] E. Locatelli, I. Monaco, M. Comes Franchini, Surface modifications of gold
562 nanorods for applications in nanomedicine, RSC Adv 5(28) (2015) 21681-21699

563 [52] L. Cavigli, M. de Angelis, F. Ratto, P. Matteini, F. Rossi, S. Centi, F. Fusi, R.
564 Pini, Size affects the stability of the photoacoustic conversion of gold nanorods, J Phys
565 Chem C 118(29) (2014) 16140-16146

566 [53] L. Cavigli, F. Ratto, F.Tatini, P. Matteini, A. Cini, I. Giovannelli, M. de
567 Angelis, F. Rossi, S. Centi, R. Pini, The influence of cellular uptake on gold nanorods
568 photostability and photoacoustic conversion efficiency, Proc SPIE 9323 (2015)
569 932346-932346

570 [54] P. G. Etchegoin, E. C. Le Ru, M. Meyer, An analytic model for the optical
571 properties of gold, J Chem Phys 125 (2006) 164705

572 [55] F. Ratto, P. Matteini, A. Cini, S. Centi, F. Rossi, F. Fusi, R. Pini, CW laser-
573 induced photothermal conversion and shape transformation of gold nanodogbones in
574 hydrated chitosan films, J Nanopart Res 13(9) (2011) 4337-4348

575 [56] B. Kemper, L. Schmidt, S. Przibilla, C. Rommel, A. Vollmer, S. Ketelhut, J.
576 Schnekenburger, G. von Bally, Influence of sample preparation and identification of
577 subcelluar structures in quantitative holographic phase contrast microscopy, SPIE
578 7715 (2010) 771504

579 [57] P. Langehanenberg, G. von Bally, B. Kemper, Autofocusing in digital
580 holography microscopy, 3D Res 2 (2011) 0100

581 [58] B. Kemper, G. von Bally, Digital holographic microscopy for life cell
582 applications and technical inspection Appl Opt 47(4) (2008) A52-A61

[59] D. Carl, B. Kemper, G. Wernicke, G. von Bally, Parameter optimized digital holographic microscope for high resolution living cell analysis, Appl Opt 43(36) (2004) 6536-6544

[60] A. E. Carpenter, T. R. Jones, M. R. Lamprecht, C. Clarke, I. H. Kang, O. Friman, D. A. Guertin, J. H. Chang, R. A. Lindquist, J. Moffat, P. Golland, D. M. Sabatini, Cell Profiler: image analysis software for identifying and quantifying cell phenotypes, Genome Biol 7(10) (2006) R100

[61] D. Bettenworth, P. Lenz, P. Krausewitz, M. Brückner, S. Ketelhut, D. Domagk, B. Kemper, Quantitative stain-free and continuous multimodal monitoring of wound healing in vitro with digital holographic microscopy, PLOS ONE 9 (2014) 07317

[62] W. Albrecht, T. S. Deng, B. Goris, M. A. van Huis, S. Bals, A. van Blaaderen, Single particle deformation and analysis of silica-coated gold nanorods before and after femtosecond laser pulse excitation, Nano Lett 16(3) (2016) 1818-1825

[63] I. Pastoriza-Santos, J. Pérez-Juste, L. M. Liz-Marzán, Silica-coating and hydrophobation of CTAB-stabilized gold nanorods, Chem Mater 18(10) (2006) 2465-2467

[64] I. E. Sendroiu, M. E. Warner, R. M. Corn, Fabrication of silica-coated gold nanorods functionalized with DNA for enhanced surface plasmon resonance imaging biosensing applications, Langmuir 25(19) (2009) 11282-11284

[65] S. O. Obare, N. R. Jana, C. J. Murphy, Preparation of polystyrene- and silica-coated gold nanorods and their use as templates for the synthesis of hollow nanotubes, Nano Lett 1(11) (2001) 601-603

[66] P. A. Buining, B. M. Humbel, A. P. Philipse, A. Verkleij, Preparation of functional silane-stabilized gold colloids in the (sub)nanometer size range, Langmuir 13(15) (1997) 3921-3926

[67] C. Li, Y. J. Li, Y. Y. Ling, Y. W. Lai, C. L. Wu, Y. B. Zhao, Exploration of the growth process of ultrathin silica shells on the surface of gold nanorods by the localized surface plasmon resonance, Nanotechnology 25(4) (2014) 045704

[68] L. M. Liz-Marzán, M. Giersig, P. Mulvaney, Sinthesis of nanosized gold-silica core-shell particles, Langmuir 12(18) (1996) 4329-4335

[69] P. Mulvaney, Surface plasmon spectroscopy of nanosized metal particles, Langmuir 12(3) (1996) 788-800

[70] C. S. Chang, L. J. Rothberg, Plasmon-enhanced photoconductivity in amorphous silicon thin films by use of thermally stable silica-coated gold nanorods, Chem Mater 27(9) (2015) 3211-3215

[71] R. Mooney, L. Roma, D. Zhao, D. Van Haute, E. Garcia, S. U. Kim, A. J. Annala, K. S. Aboody, J. M. Berlin, Neural stem cell-mediated intratumoral delivery of gold nanorods improves photothermal therapy, ACS Nano 8(12) (2014) 12450-12460

[72] Y. S. Zhang, Y. Wang, L. Wang, Y. Wang, X. Cai, C. Zhang, L. V. Wang, Y. Xia, Labeling human mesenchymal stem cells with gold nanocages for in vitro and in vivo tracking by two-photon microscopy and photoacoustic microscopy, Theranostics 3(8) (2013) 532-543

[73] L. M. Ricles, S. Y. Nam, K. Sokolov, S. Y. Emelianov, L. J. Suggs, Function of mesenchymal stem cells following loading of gold nanotracers, Int. J. Nanomed. 6 (2011) 407-416

[74] Y. Qiu, Y. Liu, L. Wang, L. Xu, R. Bai, Y. Ji, X. Wu, Y. Zhao, Y. Li, C. Chen, Surface chemistry and aspect ratio mediated cellular uptake of Au nanorods, Biomaterials 31(30) (2010) 7606-7619

[75] E. E. Connor, J. Mwamuka, A. Gole, C. J. Murphy, M. D. Wyatt, Gold nanoparticles are taken up by cells but do not cause acute cytotoxicity, Small 1(3) (2015) 325-327

[76] A. M. Alkilany, P. K. Nagaria, C. R. Hexel, T. J. Shaw, C. J. Murphy, M. D. Wyatt, Cellular uptake and cytotoxicity of gold nanorods: molecular origin of cytotoxicity and surface effects, Small 5(6) (2009) 701-708

[77] F. Zhao, Y. Zhao, Y. Liu, X. Chang, C. Chen, Y. Zhao, Cellular uptake, intracellular trafficking, and cytotoxicity of nanomaterials, Small 7(10) (2011) 1322-1337

Supporting Informations

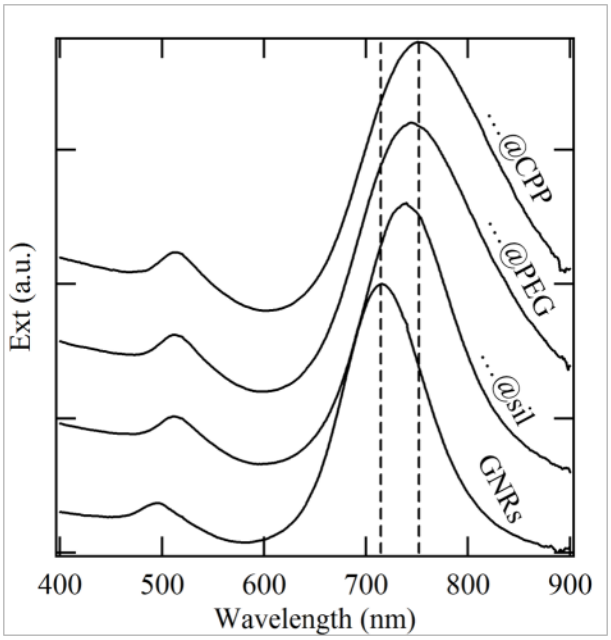

Figure S1. Spectra of optical extinction of gold nanorods (GNRs) before and after successive addition of 30 nm of organosilica, polyethylene glycol (PEG) and cell penetrating peptides (CPPs), from bottom to top. The typical plasmonic band in the far-red / near-infrared window is seen to undergo a significant redshift upon silanization. Some additional redshift and broadening is observed even after PEGylation and bio-conjugation, which may be ascribed to the interplay of the modification of the dielectric landscape and some loss of the particles in the steps of purification (eight cycles of centrifugation after silanization).

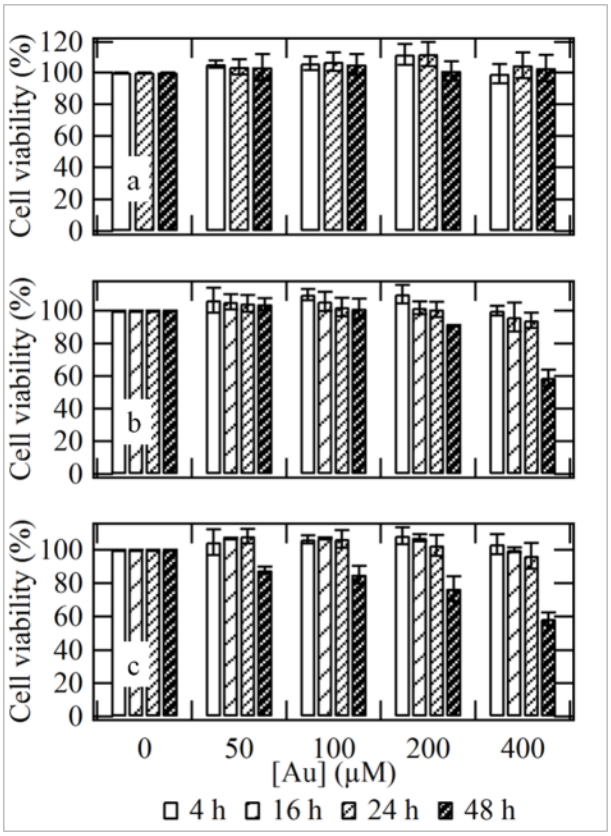

Figure S2. Evaluation of the cytotoxicity of samples S0 (***a***), S5 (***b***) and S30 (***c***) on J774A.1 macrophages by a WST-8 assay, in the concentration range between 50 to 400 μM Au and for incubation times between 4 to 48 hrs.

Samples	Damage thresholds
S0	**2.5 mJ/cm^2**
S5	**3.7 mJ/cm^2**
S30	**6.5 mJ/cm^2**

Table S1. Threshold fluence for the onset of photoinstability in a regime of optical excitation of interest for photoacoustic imaging for samples S0, S5 and S30.